https://doi.org/10.5194/egusphere-2024-3608
Preprint. Discussion started: 16 January 2025

A random forest derived 35-year snow phenology record reveals climate trends in the Yukon River Basin

Caleb G. Pan[1], Kristofer Lasko[1], John S. Kimball[2], Jinyang Du[2], Tate G. Meehan[3], Peter B. Kirchner[4], and Sean P. Griffin[1]

[1]Geospatial Research Laboratory, Engineer Research and Development Center, US Army Corp of Engineers, Alexandria, VA, 22315, USA
[2]Numerical Terradynamic Simulations Group, W.A. Franke College of Forestry & Conservation, University of Montana, Missoula, MT, 59801, USA
[3]Cold Regions Research Engineering Laboratory, Engineer Research and Development Center, US Army Corp of Engineers, Hanover, NH, 03755, USA
[4]Southwest Alaska Inventory and Monitoring Network, National Park Service, Anchorage, AK, 99501, USA

Correspondence to: Caleb G. Pan (caleb.g.pan@erdc.dren.mil)

Abstract. This study presents a 35-year snow phenology record for the Yukon River Basin (YRB), developed using a Random Forest (RF) model at a 3.125 km resolution, capturing detailed trends in snowmelt onset and snowoff. The RF model, incorporating dynamic daily variables, improves upon traditional threshold-based methods by reducing sensitivity to transient thaw events and atmospheric noise. Model evaluation against station observations yielded a mean absolute error (MAE) of 11.6 days and a root mean square error (RMSE) of 14.9 days for snowmelt onset. For snowoff, the model achieved a MAE of 18.1 days and an RMSE of 21.3 days. This approach successfully mapped snow phenology across the diverse YRB landscape, providing valuable insight into how variations in snow cover align with regional climate patterns. Challenges such as sample bias due to limited ground-based data coverage highlight the need for expanding in-situ measurements, to improve model performance further. Trend analysis segmented by two timeframes, 1988–2005 and 2006–2023, revealed distinct climate impacts on snow phenology. During 1988–2005, high snowfall and stable temperatures resulted in hastened snowmelt onset and lengthened snowmelt durations, reflecting early-season snow abundance. In contrast, from 2006–2023, warming spring and summer temperatures corresponded with progressively earlier snowmelt onset and snowoff. These shifts in snowmelt patterns align with a lengthened snow-free season, indicating increasing influence of warmer temperatures on the snowpack. This RF-derived dataset provides an essential tool for tracking climate-driven snow changes, offering insights into hydrologic and ecologic dynamics in the YRB under accelerating climate change.

1 Introduction

Snow cover and its seasonal progression, or phenology, play a crucial role in regulating the global energy budget and shaping ecosystem structure and function (Callaghan et al., 2011). These processes directly drive ecologic and hydrologic responses to seasonal variability. In the Yukon River Basin (YRB), regional warming (Ballinger et al., 2023; Rantanen et al., 2022) has reduced snow cover (Derksen and Brown, 2012), triggering widespread environmental changes. A warmer and longer snow-free season has disrupted permafrost, boosted vegetation growth, and increased ecosystem carbon uptake (Ling and Zhang, 2003; Pulliainen et al., 2017), but also enhanced regional drought and fire disturbance (Scholten et al., 2021) and led to a decline in plant diversity (Niittynen et al., 2018) and disrupted wildlife movements (Berger et al., 2018; Cosgrove et al., 2021). Seasonal snowmelt drives much of the discharge into the Yukon River and its stream networks, and the timing of this melt has

https://doi.org/10.5194/egusphere-2024-3608
Preprint. Discussion started: 16 January 2025

significant hydrologic impacts. Earlier snowmelt has heightened flood risks, intensified the spring flood pulse, and accelerated river ice breakup (Beltaos and Prowse, 2009; Lesack et al., 2014; Semmens and Ramage, 2013). These changes are reshaping the region's geomorphology and directly affecting the communities that rely on stable snow and ice conditions in the Yukon for winter travel, recreation, and harvest (Cold et al., 2020).

Enhanced monitoring and understanding of snow phenology's spatiotemporal variability are essential for assessing risks and mitigating potential impacts on Alaskan communities reliant on the Yukon River. Ground-based observations, like snow water equivalent (SWE) and snow depth measurements from SNOTEL sites, provide valuable insights into snow phenology. However, the vast landscape heterogeneity and limited ground observation locations make it challenging to forecast snow phenology reliably across large spatial scales (Bair et al., 2023). Satellite microwave remote sensing offers a valuable alternative for mapping snow phenology, especially in remote, high-latitude regions. The moderate frequency (~≤37 GHz) retrievals from operational satellite microwave radiometers are sensitive to snow cover conditions and are insensitive to clouds and low light levels, providing nearly continuous, year-round data. Importantly, the propagation of microwave energy through the snowpack is responsive to changes in snow structure, including liquid water content (LWC), grain size and density, which are key indicators of snowmelt onset (Tedesco et al., 2015). However, the sampling footprint from the passive microwave retrievals can range from ~12-25 km resolution depending on frequency and can be too coarse to capture snow spatial heterogeneity, especially in mountain environments.

In contrast, Synthetic Aperture Radar (SAR) sensors are sensitive to snow conditions and offer improved spatial resolution over microwave radiometers and scatterometers. C-band SAR data from the European Space Agency (ESA) Sentinel-1 mission has proven valuable for detecting snowmelt onset using a median minima backscatter approach, often in combination with optical-infrared remote sensing imagery (Darychuk et al., 2023; Gagliano et al., 2023; Marin et al., 2020; Nagler and Rott, 2000). The ability of SAR to detect changes in snowpack structure and LWC makes it particularly effective for identifying the onset of snowmelt, as the C-band radar backscatter at VV and VH polarizations decreases when snow transitions from dry to wet. The extraction of snowmelt onset using Sentinel-1 missions shows great promise, providing excellent detail with a spatial resolution of 10 meters. However, a current limitation of these data is the relatively short temporal record. Sentinel-1A began operations in April 2014, followed by Sentinel-1B nearly two years later in April 2016. Unfortunately, Sentinel-1B was decommissioned in December 2021 due to power issues. While higher-frequency K-band and Ka-band radiometers are limited by their coarser spatial resolution, they provide twice-daily acquisitions for polar latitudes from 1988 to the present, offering a valuable long-term data record.

Several snow phenology algorithms utilize K- and Ka-band radiometric brightness temperature (Tb) measurements collected from the Defense Meteorological Satellite Program (DMSP) Special Sensor Microwave Imager (SSM/I) (1987-present) and Special Sensor Microwave Imager/Sounder (SSMIS) (2004-present). Various retrieval algorithms using these data to derive

https://doi.org/10.5194/egusphere-2024-3608
Preprint. Discussion started: 16 January 2025

snow properties include: 1) the Tb diurnal amplitude variation (DAV) method (Ramage and Isacks, 2002; Tedesco and Miller, 2007), 2) the Tb differencing approach (K-Ka) (Wang et al., 2013, 2016), 3) the use of a single frequency Tb temporal change algorithm coupled with reanalysis surface temperature (Kim et al., 2017), 4) the gradient ratio polarization (GRP) approach (Dolant et al., 2016; Pan et al., 2018) and 5) a remote sensing and physics-based hybrid method (Dattler et al., 2024). Each algorithm leverages the interaction between the surface snowpack, its liquid water content (LWC), and the resulting effect on the Tb signal at each band or polarization. Specifically, dry snow conditions lead to volumetric scattering in both K and Ka bands, with stronger scattering at higher frequencies. In contrast, when the LWC within the snowpack increases, the microwave signal is attenuated, resulting in a decrease in microwave backscatter at both bands (Tedesco et al., 2015). Due to these interactions, past algorithms have successfully derived snow phenology by analyzing Tb time series using these approaches and applying thresholds to identify transitioning snow conditions.

While threshold-based methods have successfully predicted snow phenology, they often fail to fully capture landscape variability in snow conditions due to their coarse spatial resolution. Additionally, these methods are susceptible to atmospheric noise, which can lead to potential false positives. Alternatively, machine learning (ML) offers a flexible empirical modeling approach for estimating snow properties from satellite observations and other ancillary data. ML provides the ability to model complex interactions across diverse datasets and has been applied widely in cryosphere applications (Campbell et al., 2021; Dunmire et al., 2024; Guidicelli et al., 2023; Tedesco et al., 2004; Tsai et al., 2019). Among ML methods, random forest (RF) has demonstrated success, often bettering other methods, due to its flexibility, ability to handle high-dimensional data, and success in handling complex environmental datasets. RF constructs multiple decision trees during training and aggregates their outputs, reducing overfitting and increasing robustness in diverse datasets. Furthermore, RF can manage missing data and maintain accuracy even with uncorrelated features (Breiman, 2001).

Our study integrates a temporal component into the RF framework, allowing the model to capture seasonal variations in snow cover. Unlike traditional thresholding methods that rely on fixed values (Pan et al., 2021), the RF model accounts for multiple variables and their interactions, producing more nuanced predictions. By incorporating time-series data, our RF model tracks the evolution of snow conditions throughout the season (Rittger et al., 2021), improving predictions of snowmelt onset.

In this paper, we examine the question: How amplified Arctic warming has influenced the timing, duration, and variability in snow phenology in the YRB? To address this question, we use an ML framework informed with Tb time series from the K- and Ka-bands collected from SSM/I(S), along with other complimentary dynamic and static variables, to estimate primary spring snowmelt onset and snowoff dates across the YRB from 1988 to 2023. The resulting annual snow phenology maps are produced at an enhanced resolution of 3.125 km, offering an improvement over previous records derived directly from passive microwave observations and enabling a more detailed delineation of landscape heterogeneity. We then apply the snow phenology outputs with other ancillary and in-situ environmental data to: 1) assess model performance and define relative quality maps, 2) examine YRB snow phenology climatology and compare it with anomalous years, 3) analyze spatiotemporal

https://doi.org/10.5194/egusphere-2024-3608
Preprint. Discussion started: 16 January 2025

trends in snow phenology over the period of record, and 4) explore interactions between snow phenology and seasonal snowfall and temperature trends.

2 Study Area

The YRB constitutes one of North America's largest river basins (Figure 1). This region experiences six to nine months of snow cover annually, and spring snowmelt runoff is the main hydrologic contribution to the discharge (Brown et al., 2020). The YRB has a mean annual discharge of 6400 $m^3 s^{-1}$ (Brabets et al., 2000), with a drainage area exceeding 853,300 km^2 and covers 10 degrees of latitude from 59°N to 69°N, extends into the Canadian Yukon and British Columbia territories to the east, and the west coast of Alaska before draining into the Bering Sea. The diverse topography, with a median elevation of 617 m and extending from sea level to the highest elevations of the Brooks (2735 m) and Alaska (6190 m) Ranges, encompasses a diversity of northern boreal, arctic, alpine and maritime biomes. Evergreen needleleaf forests are the dominant vegetation cover (54%) followed by broadleaf deciduous forests (9%) covering the valley bottoms and into the mid-elevations. The Yukon Delta and higher elevations have tall and low shrubs (9%) mixed with some dry and wet herbaceous (9%) tundra as the dominant plant community. Permafrost is present to a large extent in the YRB, and comprises several types including sporadic (14%), discontinuous (46%) and continuous (16%) and moderately thick to thin permafrost (24%) (Brabets et al., 2000). Historically the Yukon River served as the main travel corridor of the region and YRB is the ancestral homelands of several Native Alaskan culture. Presently, many communities are inextricably linked to and rely upon the Yukon and its tributaries for travel, subsistence, and livelihood (Cold et al., 2020).

https://doi.org/10.5194/egusphere-2024-3608
Preprint. Discussion started: 16 January 2025

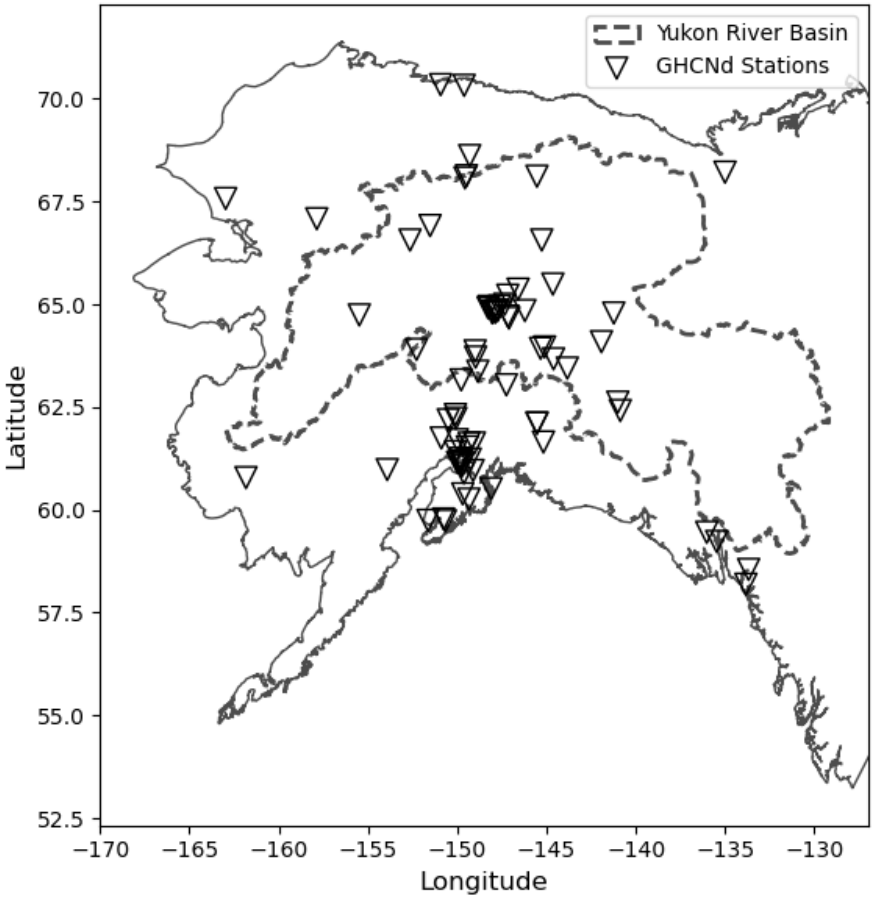

125

Figure 1: The Alaska study area, the YRB boundary is delineated by the dashed black polygon and the black upside-down triangles indicate climate stations utilized for creating a training and testing dataset for our ML models.

3 Data

3.1 Training and Testing Datasets

130 We acquired daily in situ snow depth measurements from the Global Historical Climatology Network (GHCNd) (Menne et al., 2012) to build the RF model training and testing dataset. Filtering stations across Alaska, 77 stations included snow depth measurements spanning at least one year between 1988 and 2023. Although many researchers use the day of peak SWE or a breakpoint after peak SWE to determine the onset of snowmelt (Darychuk et al., 2023; Gagliano et al., 2023), the lack of SWE measurements in the GHCNd led us to use peak snow depth instead. Specifically, for each station and year, we identified
135 snowmelt onset by locating the day with the highest snow depth in spring (Mar-May). However, peak snow depth often did not accurately represent the true onset of snowmelt, as decreases in snow depth can occur due to factors like wind redistribution,

https://doi.org/10.5194/egusphere-2024-3608
Preprint. Discussion started: 16 January 2025

sublimation, or compaction, unrelated to snowmelt. For this reason, we could not apply rigid rules to defining snowmelt onset using snow depth.

To improve the identification of snowmelt onset, analysts used their best judgment, supported by air temperature data. When average daily temperatures consistently rose above freezing and snow depth began to steadily decrease from its peak, it became easier to pinpoint the onset of snowmelt. Identifying snowoff from snow depth was more straightforward and defined as the first day when snow depth reached 0 for at least 10 consecutive days in spring. After analyzing each in situ snow depth time series, we compiled 971 observations for snowmelt onset and 933 snowoff observations for RF training and testing.

3.2 Timeseries Datasets

In this study, we employ a combination of dynamic and static datasets as RF model predictors and for analyzing the model snow phenology outputs. The dynamic RF predictors include the Tb-derived indices, Tb Difference (TBD) and Gradient Ratio Polarization (GRP), as well as their respective 3-day moving averages (MA_TBD and MA_GRP). We also utilize daily Thaw Degree Days (TDD), day of year (DOY), and daily snow cover. Together, these dynamic datasets provide a comprehensive basis for capturing both seasonal and interannual variability in snow phenology.

We also include several static landscape factors and assess how landscape features influence model sensitivity. Static variables include Fractional Water (FW), Fraction Tree Cover (TC), elevation (GTOPO), aspect, and proximity, described by a pixel's proximity to the nearest ocean. These datasets are summarized in Table 1 and a comprehensive table with all datasets used in this study are found in Table A1.

Table 1: Dynamic and static predictor summary, including their abbreviation, spatial and temporal resolutions.

Dataset	Spatial Resolution	Temporal Resolution
Tb Difference (TBD)	3.125 km	daily
Gradient Ratio Polarization (GRP)	3.125 km	daily
Moving Average TBD (MA_TBD)	3.125 km	3-day moving average
Moving Average GRP (MA_GRP)	3.125 km	3-day moving average
Cumulative Thaw Degree Day (TDD)	1 km	daily
Day of Year (DOY)		daily
Snow covered area	4 km and 3 km	daily
Fraction Water (FW)	1 km	static
Tree Cover (TC)	250 m	static
Elevation (GTOPO)	1 km	static
Aspect	1 km	static
Proximity	1 km	static

https://doi.org/10.5194/egusphere-2024-3608
Preprint. Discussion started: 16 January 2025

3.2.1 Passive Microwave Satellite Record

We acquired K-band (19 GHz) and Ka-band (37 GHz) afternoon Tb retrievals at vertical (V) and horizontal (H) polarizations from the MEaSUREs Calibrated Enhanced Resolution Passive Microwave Daily EASE-Grid 2.0 Brightness Temperature ESDR, available from the National Snow and Ice Data Center (NSIDC) (Brodzik and Long, 2016). This Tb record is multidecadal and calibrated across multiple sensors and platforms from different frequencies and polarizations from the NOAA DMSP SSM/I and SSMIS. Each platform has several sensors, from SSMI/I we selected F08 (1998-1991), F11 (1992-1995), F13 (1996-2007) and from SSMIS we used F17 (2007-2016) and F18 (2017-2023). These sensors were selected because their equatorial overpass time remained consistent while in commission. Missing temporal observations were gap-filled using a temporal linear interpolation of adjacent Tb retrievals (Wang et al., 2016).

Native sampling resolution of the combined K and Ka Tb retrievals are ~25 km or coarser, however the MEaSUREs products used were processed using the scatterometer image reconstruction (SIR) approach to obtain an enhanced spatial grid resolution of 6.25 km (K) and 3.125 km (Ka) from the overlapping Tb antenna patterns (Brodzik et al., 2018; Long and Brodzik, 2016). We then resampled K-band Tb retrievals to match the Ka resolution of 3.125 km using a nearest neighbor interpolation.
We then reduce the vertically polarized K and Ka bands into a Tb difference index, henceforth described as TBD, defined as the difference between K and Ka bands (Wang et al., 2013). We also reduce the K and Ka bands into an additional index, the GRP by first calculating the Gradient Ratio (GR) at vertical and horizontal polarizations using equation 1 (Grenfell and Putkonen, 2008):

$$GR\left(pol_{(37,19)}\right) = \frac{[T_b\ (pol, 37) - T_b\ (pol, 19)]}{[T_b\ (pol, 37) + T_b\ (pol, 19)]}$$

The GRP is then ratioed using equation 2 (Dolant et al., 2016):

$$GRP = \frac{GR_V}{GR_H}$$

Together, both the TBD and GRP provide a source for identifying daily snow conditions such as dry and stable, melting, and disappeared (Pan et al., 2020; Wang et al., 2016).

3.2.2 Daily Snow Cover

We use ancillary daily snow covered area estimates to determine the presence or absence of snow at a given location and time. For the period from 1988 to 2023, we relied on two data sources. From 2004 to 2023, we used the Interactive Multisensor Snow and Ice Mapping System (IMS) daily snow cover extent record, which has a 4 km resolution. The IMS provides global coverage and is informed by expert interpretation of geostationary visible satellite imagery, polar-orbiting multispectral satellite sensors, PMW sensors, and ground observations (Helfrich et al., 2007). Although the IMS also provides daily snow cover area outputs at a coarser 24 km resolution dating back to 1997, we opted to use alternative higher spatial resolution snow

https://doi.org/10.5194/egusphere-2024-3608
Preprint. Discussion started: 16 January 2025

cover estimates from SnowModel (Liston et al., 2020) to fill in the earlier years (1988–2003), as the 24 km resolution IMS data is less able to resolve snow cover heterogeneity in complex terrain and does not cover the entire period of interest.

The SnowModel provides daily estimates of snow properties for the North American domain at a 3 km resolution from 1980 to 2020 (Liston et al., 2023, Liston et al., 2020). Although SnowModel includes several snow variables, we used the modeled snow depth to define daily snow presence or absence. Specifically, if the estimated snow depth exceeded 0 on any given day, we assigned a value of 1; if snow depth was 0, we assigned a value of 0.

3.2.3 Daymet

We calculated daily cumulative thaw degree days (TDD) using the North American Daymet (V4) record (Thornton et al., 2021). We obtained the Daymet data through the Microsoft Planetary Computer STAC, which is produced by the Oak Ridge National Laboratory DAAC. Daymet provides 1 km spatial resolution, interpolated from daily weather station temperature observations, but with potential bias introduced from the sparse regional weather station network, especially at higher elevations. TDD serves as a useful proxy for assessing the amount of incoming solar radiation the snowpack has been exposed to at a given location and reflects the seasonal dynamics of anomalous temperatures that influence snowmelt onset.

3.3 Static Datasets

We also used several static datasets for model training and to examine the influence of land cover on snow phenology prediction. We represented elevation using the GTOPO30 dataset at a 1 km resolution and used it to derive terrain aspect. We acquired average fractional water inundation (FW) from the global land parameter data record, generated from the Advanced Microwave Scanning Radiometer for EOS and the Advanced Microwave Scanning Radiometer 2 records (Du et al., 2017). In addition to prediction and assessing uncertainty, FW served as a mask to screen model outputs likely affected by water contamination.

To represent percent tree cover (TC), we utilized the MODIS MOD44B V005 500m Vegetation Continuous Fields product. Additionally, we created a custom dataset, termed ‘proximity,’ which captures the distance of each pixel from the ocean. This is important because Tb pixels near large water bodies are prone to water contamination and frequent cyclonic events that can influence LWC in the regional snowpack (Rees et al., 2010).

3.4 Ancillary Datasets

We used an established satellite-based snow phenology dataset for comparison with our ML results. These data include the annual timing (DOY) of snowmelt onset and snowoff for the YRB from 1988 to 2018 mapped to a 6.25 km resolution grid (Pan et al., 2020, 2021). The data were also derived using a similar thresholding approach of the GRP and TBD derived from microwave Tb observations. Additionally, a glacier land cover dataset for the YRB was obtained from the Glacier Covered

https://doi.org/10.5194/egusphere-2024-3608
Preprint. Discussion started: 16 January 2025

Area for the State of Alaska dataset (Roberts-Pierel et al., 2022), which we used to identify pixels that maintain year-round snow cover, as they do not experience a 'snowoff.'

4 Methods

4.1 RF Framework

We implemented a RF classifier to predict snow phenology, specifically focusing on estimating the annual timing (day of year) of snowmelt onset and snowoff across the YRB. The RF approach was chosen due to its ability to handle complex, high-dimensional data, and robustness to overfitting, making it well-suited for cryosphere applications (Breiman 2001, Alifu et al., 2020; Blandini et al., 2023). Although RF does not inherently model temporal sequences like some other algorithms, temporal dimensions were incorporated by structuring each day as a sample within a sequential framework. Accordingly, we used the RF implementation in scikit-learn (Pedregosa et al., 2011).

In this study, the RF model snow phenology metrics were derived at 3.125 km resolution from 1988-2023, which represents a significant spatial and temporal enhancement over other similar snow records developed for the YRB (Pan et al. 2020). Although the original K-band Tb data resolution was 6.25 km, the 3.125 km resolution of the RF predictions is more consistent with the native resolution of the Ka-band Tb record, which are critical for capturing snowpack characteristics. Additionally, the 3.125 km resolution is approximate to—or still coarser than—other RF model predictor datasets used, which helps to ensure spatial coherence in representing landscape heterogeneity.

4.1.1 RF Model Setup

To enhance the prediction of snow phenology, we configured the RF model to delineate daily snow conditions. We did this by classifying expected snow conditions for each day in a timeseries leading up to the observed snowmelt onset or snowoff day in spring as either 'dry snow' or 'present.' After the observed onset or snowoff day, the conditions are labeled as 'wet snow' or 'absent', respectively. By labeling the timeseries accordingly, we were able to: 1) add a temporal dimension to the RF classifier, 2) expand the RF training and testing datasets, and 3) use the day each labeled timeseries changes as the snow phenology date (Figure 2).

https://doi.org/10.5194/egusphere-2024-3608
Preprint. Discussion started: 16 January 2025

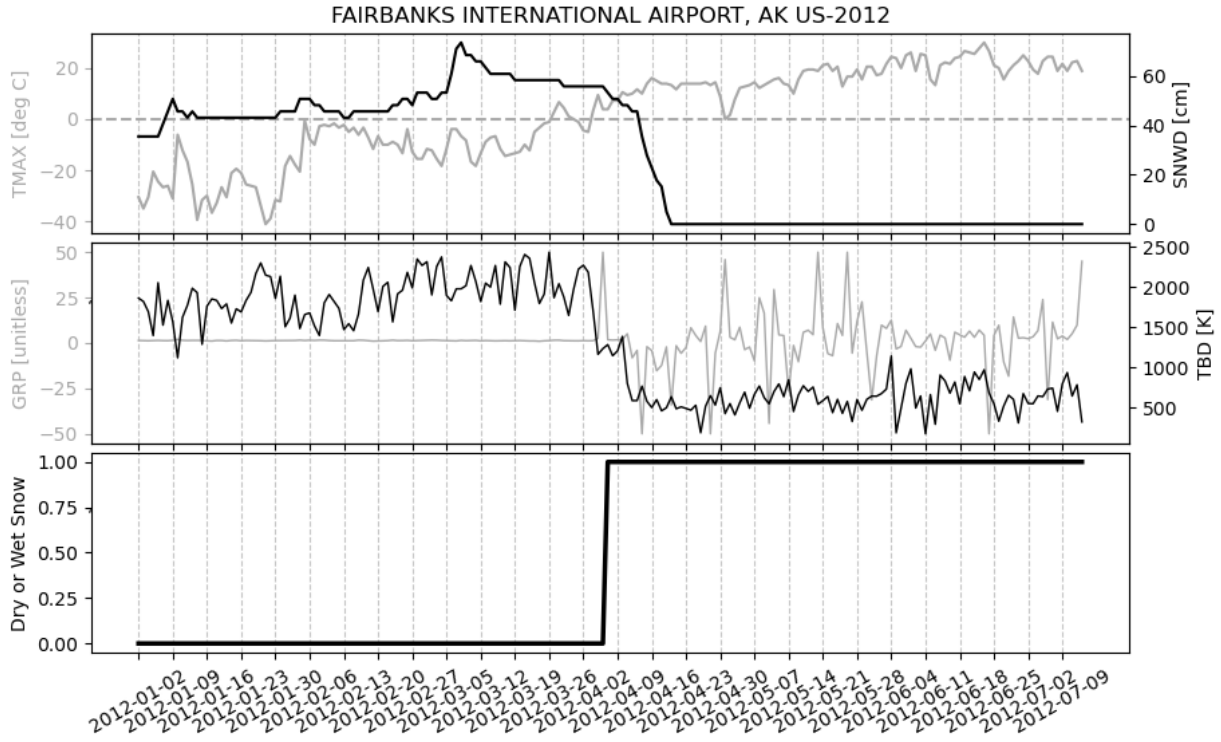

Figure 2: Comparison between daily in situ air temperature and snow depth measurements (top plot) taken from Fairbanks International Airport in 2012 and collocated brightness temperature derived TBD and GRP (middle plot). The bottom plot shows the daily snowmelt onset RF model output. The snowmelt onset, marked by the transition from dry to wet snow, is identified as the day when the model output changes from 0 to 1.

To assess daily snow conditions, each model was trained using a set of daily and static predictors. Daily predictors included TDD, TBD, GRP, and Day of Year (DOY). Static predictors, representing landscape and environmental characteristics, included proximity to oceans, TC, FW, elevation, and aspect. All static variables were scaled from 0 to 1. Table 1 includes more detail on the model training datasets. Snowoff included snowmelt onset as a predictor with the intention that this variable would ensure that snowoff predictions would occur after the snowmelt onset.

We parameterized the RF models using a cross-validated grid search method. This approach systematically evaluates various combinations of hyperparameters to identify the best configuration by performing cross-validation. It selects the combination of parameters that minimizes the user-defined evaluation metric, such as the cross-validated score (Jääskeläinen et al., 2022). The grid of adjustable parameters we provided for hyper-tuning included the number of the RF decision trees, the maximum depth of each tree, the minimum sample size for node splitting, the minimum sample size for leaf nodes, and the maximum number of features considered at each split. In addition to parameter selection, the cross-validated score also helps minimize overfitting.

https://doi.org/10.5194/egusphere-2024-3608
Preprint. Discussion started: 16 January 2025

Finally, we identified the timing of snowmelt onset and snowoff from the model outputs by applying a logic that returned the first day of 10 consecutive days classified as either 'wet snow' or 'absent.'

4.1.2 Assessing Uncertainty and Error

Model performance was assessed using a bootstrapping approach, with an 80/20 split between training and testing data, with replacement, allowing us to evaluate model accuracy and variability. For each bootstrap iteration, performance was evaluated with the training data by 1) extracting the R^2 value to quantify the agreement between observed and predicted dates, and 2) aggregating the Mean Absolute Error (MAE) across different land cover types. To determine whether differences in model error across land cover characteristics were statistically significant, we applied a one-way Analysis of Variance (ANOVA). For each iteration, we also calculated feature importance, determining the average importance and standard deviation for each feature.

The output absolute error from our model bootstrapping was used as the dependent variable in an ordinary least squares (OLS) regression, with land cover variables such as FW, TC, elevation, aspect, and proximity serving as the explanatory variables (Kim et al., 2011). The goal was to establish a relationship between the observed error and the land cover characteristics to identify pixels in the YRB where we may expect lower or higher errors. We then applied the OLS model across the YRB to predict anticipated error. These values were scaled from 0 to 1, creating a dimensionless quality control (QC) metric. The QC metric was further classified into natural breaks, with qualitative labels of 'Best', 'Good,' 'Moderate,' and 'Low' to describe the relative quality of the model predictions.

4.2 Trend Analysis

4.2.1 Snow Phenology

To analyze snow phenology trends over time, we developed snow phenology climatologies for the period 1991–2020. Using a natural break classification method, we divided the data into two categories: 'earlier' and 'later' snow events. These two classes represented pixels in the YRB that experienced respective earlier or later snow events in each year of record, relative to their climatological mean value for each pixel. Next, for each year, we classified the snow metrics using the same two categories derived from the climatology and calculated the annual change in area for each class. If the area of the 'earlier' class decreased, we expected a corresponding increase in the 'later' class. To assess the trends over time, we applied a linear regression and performed a Mann-Kendall Test (MKT) to evaluate the direction and strength of the annual changes in area.

https://doi.org/10.5194/egusphere-2024-3608
Preprint. Discussion started: 16 January 2025

4.2.2 Temperature and Snow Depth

Seasonal air temperature across the YRB was analyzed using data from GHCNd climate stations. To create a single, harmonized air temperature time series, we selected stations with at least 17 years of data for each of the two time periods (1988–2005 and 2006–2023) from an initial set of 35 stations in the YRB. This selection criterion reduced the set to 8 stations for 1988–2005 and 15 stations for 2006–2023. With the selected stations, we then calculated seasonal average temperature time series for each period, specifically for winter, spring, summer, and combined spring/summer temperatures.

We also extracted the snow depth at the day of snowmelt onset across YRB using the GHCNd climate stations. Like temperature, we required a station to have recorded at least 17 years of snow depth. We also checked each of these stations, to determine if the annual snow depth measurements were complete because they are often incomplete. These screening criteria resulted in 4 stations selected for 1988-2005 and 13 stations for 2006-2023.

5 Results

5.1 RF Model Performance

The RF model effectively classified daily snow conditions for both snowmelt onset and snowoff, as demonstrated by the bootstrapped results. For snowmelt onset, the model classified snow conditions as either 'dry snow' or 'wet snow' with high accuracy. The model achieved an F1-score, precision, and recall averaging 0.97, indicating a strong ability to balance false positives and false negatives. These metrics suggest that the RF model reliably distinguished between dry and wet snow conditions leading up to snowmelt onset. Gridsearch results for the RF are found in Table A2.

Similarly, for snowoff, the RF model successfully classified daily snow conditions as either 'present' or 'absent'. The model maintained an average F1-score, precision, and recall of 0.96. This consistent performance highlights the model's ability to accurately capture the transition between snow presence and absence throughout the snowoff period, providing dependable predictions of snow cover dynamics.

Once the snowmelt onset and snowoff days of year (DOY) were extracted, they were compared against our testing data generated during bootstrap iterations. In each iteration, an 80/20 (training/testing) split ensured that the testing data represented a unique subset of high-quality observations from different years and locations, allowing the model's generalizability to be evaluated across a variety of conditions. The bootstrapped results yielded an R^2 of 0.72 for snowmelt onset and 0.83 for snowoff, demonstrating that the predicted snow DOY metrics closely matched the observed values from the testing data. Additionally, the model produced a Mean Absolute Error (MAE) of 5.86 [days] for snowmelt onset and 5.18 [days] for snowoff, indicating the average deviation between the predicted and observed dates. The Root Mean Square Error (RMSE) values of the model results were 8.07 [days] for snowmelt onset and 6.89 [days] for snowoff. Overall, these metrics indicate favorable model performance in predicting the timing of these key snow phenology events across the YRB.

https://doi.org/10.5194/egusphere-2024-3608
Preprint. Discussion started: 16 January 2025

The final error assigned to the snow phenology dataset is assessed by comparing the RF model outputs on the full YRB dataset with the additional training dataset derived from the limited number of GHCNd stations within the YRB. From these stations we calculated a MAE 11.6 [days] and RMSE of 14.9 [days] to the snowmelt onset product. The model snowoff results showed a MAE of 18.1 [days] and RMSE of 21.3 [days] relative to the station observations. The higher final observed errors compared to the bootstrapped errors are likely attributed to the greater variability in land cover, which is not fully represented by the in-situ ground stations.

5.1.1 Model Feature Importance

On average, the most influential features for predicting snowmelt onset were DOY, TDD, snow cover presence and TBD, in that order (Fig. A3). The snowoff predictions followed a similar pattern, with TDD, DOY, snow cover presence, and TBD emerging as the top-ranked features (Fig. A4). In both models, the dynamic, time-series features—such as temperature and snow cover presence—played a significantly larger role in the predictions compared to the static features, such as proximity, elevation, and fractional water cover. Interestingly, the GRP had relatively low importance for the snowoff model, which is likely due to its erratic behavior during no snow conditions and vegetation.

5.1.2 Landcover and Uncertainty

Mean absolute errors were binned by land cover to assess whether land cover characteristics had a significant influence on model performance. Land cover features such as elevation, TC, aspect, proximity, and FW were grouped into four natural breaks and compared with the corresponding model MAE to identify potential patterns or relationships. Figures 3 and 4 indicate that when elevation, proximity and FW decrease, MAE also decreases for both snowmelt onset and snowoff predictions. Conversely, as TC increases, MAE also increases, though this is only observable for snowmelt onset predictions. Also notable is that higher FW is associated with much higher MAE values for snowmelt onset. Hence, FW may be a major factor behind the overall lower model performance, relative to snowoff. Yet, overall, these landcover and error interactions are as anticipated – error increases with higher surface water cover, coastal proximity, and tree cover.

https://doi.org/10.5194/egusphere-2024-3608
Preprint. Discussion started: 16 January 2025

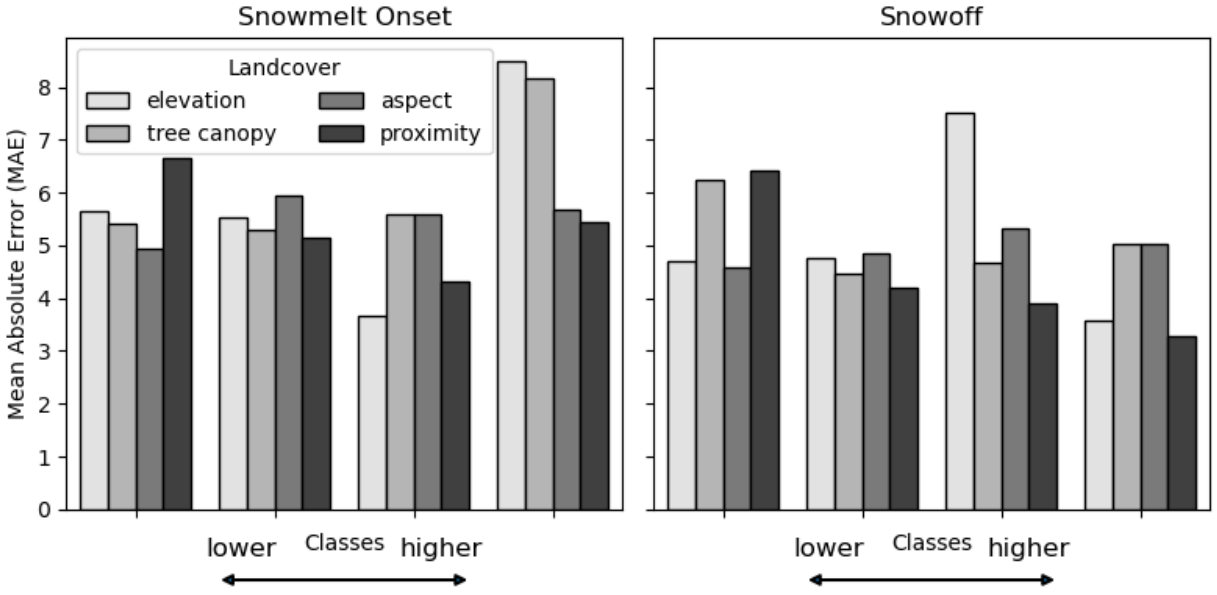

Figure 3: Average snowmelt onset (left) and snowoff (right) MAE aggregated by landcover. Landcover was binned using a Jenks classification with lower values on the left and higher values moving to the right.

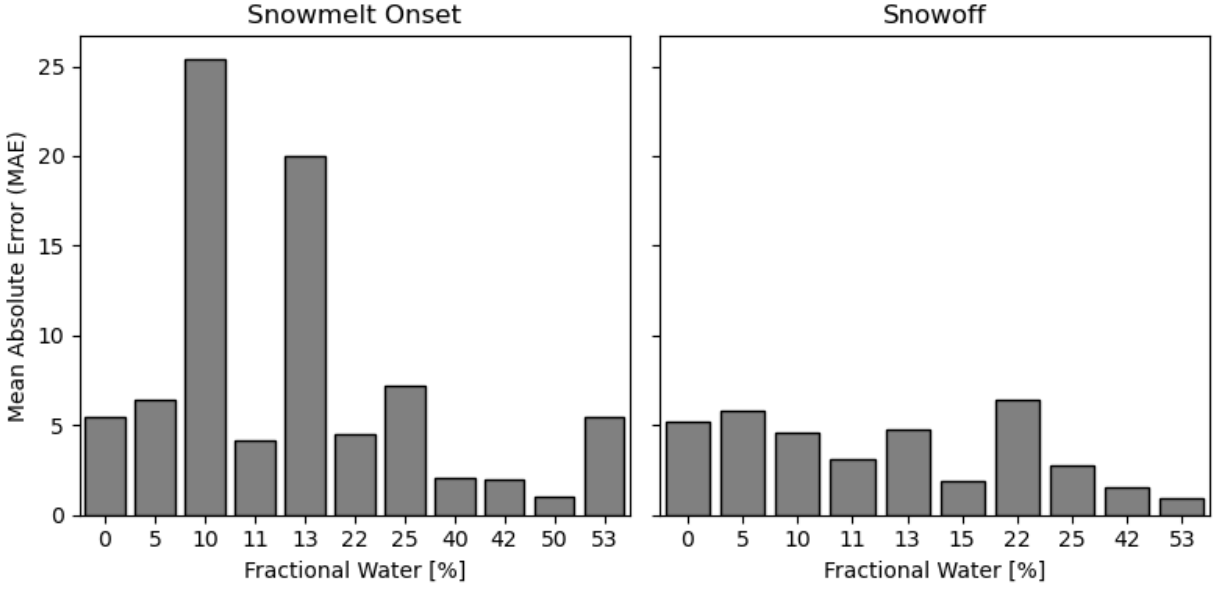

Figure 4: Average snowmelt onset (left) and snowoff (right) MAE aggregated by FW.

The one-way ANOVA results indicate that each land cover characteristic has a significant ($p<0.0001$) influence on MAE. For both snowmelt onset and snowoff, FW had the greatest impact with an F-statistic = 40.63. TC and proximity also showed

https://doi.org/10.5194/egusphere-2024-3608
Preprint. Discussion started: 16 January 2025

substantial effects on MAE, with F-statistics of 21.34 and 30.18 for TC, and 10.25 and 19.22 for proximity, for snowmelt onset and snowoff, respectively. These results support inclusion of the static variables as additional RF predictors, despite their relatively low importance.

5.2 Model Comparisons

5.2.1 RF and Threshold Comparison

A comparison between the annual median snowmelt onset and snowoff dates derived from the RF model and the previous snow phenology record from Pan et al. 2020 is presented in Figure 5. For snowmelt onset, the results show a moderate correlation between the two records for the YRB, with an r-value of 0.54 ($p<0.05$). However, the previous record was derived using a Tb thresholding method and consistently predicted earlier snowmelt onset dates, averaging about 3 days earlier than our RF model. When compared to the in-situ testing dataset within the YRB, the previous snow record produced a MAE of 11 days and a RMSE of 14.57 days, like our RF model performance.

For snowoff, the two records displayed a stronger correlation, with an r-value of 0.81 ($p<0.05$). The previous approach still predicted earlier snowoff dates, with an average of Day 137, about 5 days earlier than the RF-derived snowoff. Despite the stronger correlation, the thresholding approach returned a high MAE of 32 days and an RMSE of 54 days, which is about double the error derived for the RF method. The RF-derived snowmelt onset and snowoff exhibit significantly lower standard

https://doi.org/10.5194/egusphere-2024-3608
Preprint. Discussion started: 16 January 2025

deviations compared to the previous approach, indicating that the ML method is less susceptible to outliers.

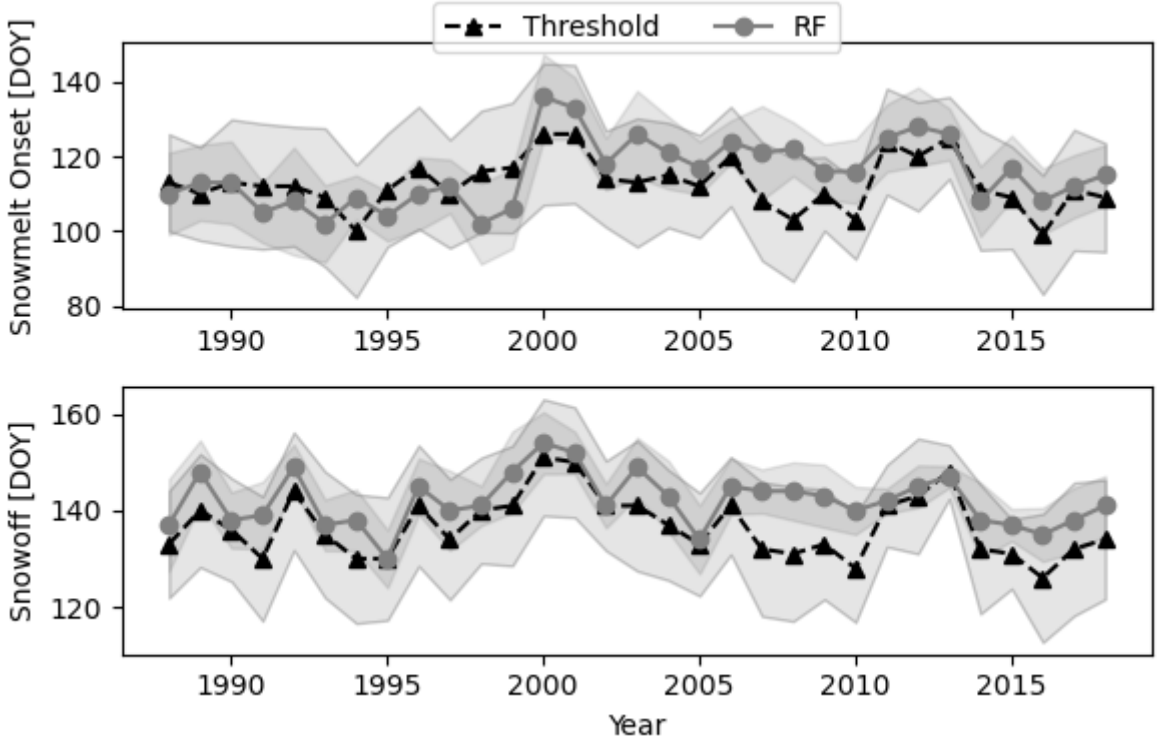

Figure 5: 1988-2018 annual median dates +/- one standard deviation for snowmelt onset (top) and snowoff (bottom) for the ABoVE GRP threshold model (Pan et al. 2020) (black triangles) and the RF model (this study) (grey circles).

5.2.2 Snowoff Model Comparison

Our snowoff predictions incorporate two different modeled snow cover datasets, IMS and SnowModel, because no dataset alone spans our full period of record; both datasets were used as features in the RF model. Specifically, we used the 4 km IMS dataset (2004-2023) and the 3 km SnowModel (1988-2003) to calculate annual snowoff using a 10-day moving window. We then evaluated these outputs against the YRB training dataset to assess their performance relative to the RF results. For the period from 1997-2023, the IMS dataset achieved a Mean Absolute Error (MAE) of 15.87 days and a Root Mean Square Error (RMSE) of 21 days. During this same period, the RF-based snowoff dataset achieved a MAE of 16.03 days and an RMSE of 19.2 days.

For the earlier period (1988-1996), the SnowModel dataset produced a MAE of 13.6 days and an RMSE of 16.42 days. In comparison, the RF snowoff dataset during this period produced a MAE of 18.56 days and an RMSE of 21.2 days. These results reflect the performance of each dataset over their respective timeframes and provide insight into the reliability of the

https://doi.org/10.5194/egusphere-2024-3608
Preprint. Discussion started: 16 January 2025

RF-based snowoff model across different periods. Both IMS and SnowModel exhibited lower errors, likely due to snow cover being ranked third in feature importance within the RF model.

5.3 QAQC Maps

The QAQC maps provide a discrete qualitative index for assessing model output quality. For the snowmelt onset QAQC map, 21% of the pixels were classified as 'Best,' 38% as 'Good,' 32% as 'Moderate,' and 9% as 'Low' (Figure 6). Quantitatively, using the bootstrapped error results, these categories correspond to different error ranges: 'Best' has an error of less than 4 days, 'Good' ranges from 4 to 5 days, 'Moderate' from 5 to 7 days, and 'Low' indicates an error greater than 10 days.

The land cover derived QAQC map for snowmelt onset identified the upper headwaters of the YRB as the principal offender of model quality. This is likely because of the large lakes in the region as well as the proximity to the ocean, bringing in periodic storm systems, introducing LWC to the surface snowpack.

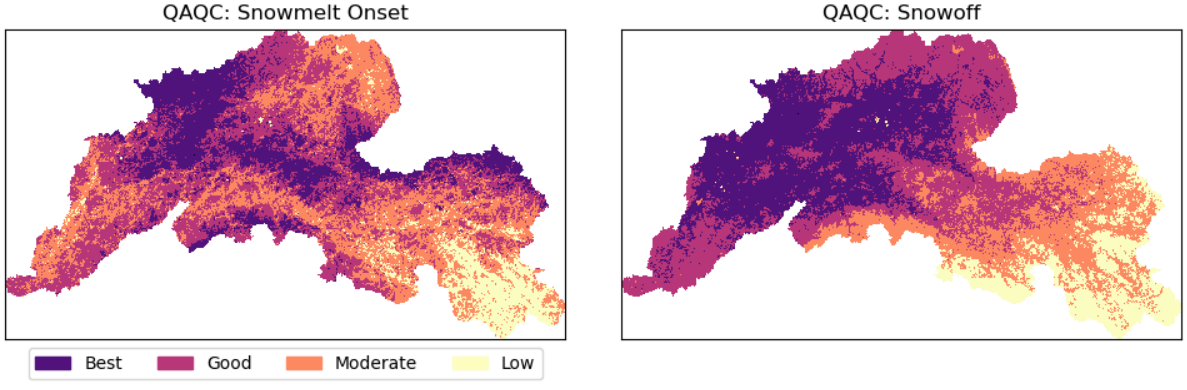

Figure 6: Snowmelt onset (left) and snowoff (right) QAQC maps were developed to identify regions of relative high to low quality classification results in relation to landcover characteristics.

For snowoff, the error distributions are similar, though the class sizes differ slightly. In the snowoff QAQC map, 'Best' covers 32% of the pixels with an error of less than 4 days, 'Good' accounts for 34% with an error between 4 and 6 days, 'Moderate' includes 22% with an error range of 7 to 11 days, and 'Low' comprises 13% of the pixels with an error greater than 11 days. The snowoff QAQC map also identified the upper headwaters of the YRB as a problematic area for model quality. However, lower quality pixels seem to be more focused at higher elevations and ridgelines. Given that snow cover at higher elevations can linger extended periods of time and even through the summer months, it is not a surprise that these pixels are ranked as 'low.' The OLS models explained 21% and 27% of the variability in error for snowmelt onset and snowoff, respectively. The relatively low explanatory power is likely due to the testing data not fully capturing the landscape heterogeneity across the YRB.

https://doi.org/10.5194/egusphere-2024-3608
Preprint. Discussion started: 16 January 2025

5.4 Snow Phenology Climatology, Anomalies, and Trends

5.4.1 Climatology of Snowmelt Onset, Snowoff, and Snowmelt Duration

The climatology of snow phenology metrics—snowmelt onset, snowoff, and snowmelt duration—offers valuable insights into seasonal patterns across the YRB, where snow phenology shows later snowmelt onset, snowoff and duration in headwaters and higher elevations and earlier dates at lower elevations and valley bottoms (Figure 7). On average, snowmelt onset (MMOD) occurs around DOY 117 ± 7.4 (~26 April), with the earliest onset recorded on DOY 100 (~9 April) and the latest on DOY 137 (~16 May). Snowoff typically occurs around DOY 142 ± 4.5 (~21 May), with the earliest snowoff observed around DOY 131 (~10 May) and the latest on DOY 160 (~7 June). The snowmelt duration, defined as the period between snowmelt onset and snowoff, spans approximately 25 ± 4.8 days.

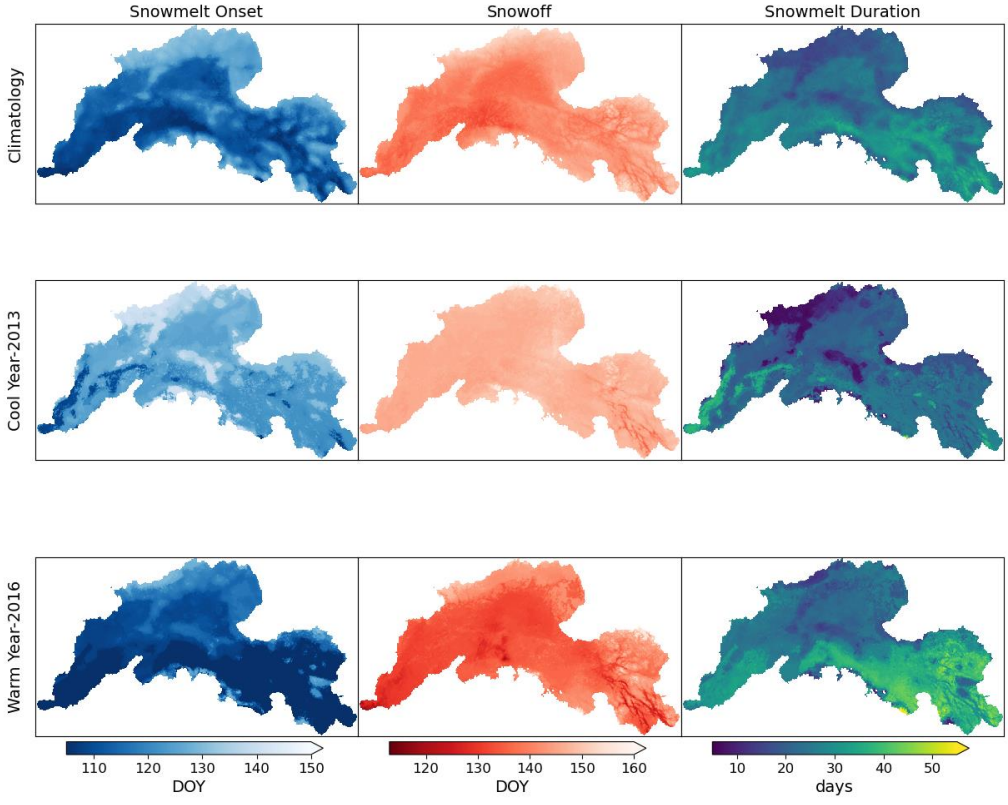

Figure 7: Climatologies produced for snowmelt onset (left), snowoff (middle) and snowmelt duration (right) for the years 1991-2020 on the top row. Middle and bottom row include the snow phenology for the years 2013 and 2016.

5.4.2 Anomalous Years

Several anomalous years in snow phenology stand out, deviating from the climatological averages. In 2016, a record-breaking warm year (Walsh et al., 2017), snowmelt onset occurred ~9 days earlier than average, and snowoff 6 days earlier, lengthening snowmelt duration by 4 days beyond the mean. Conversely, in 2013, a cooler year, snowmelt onset was 10 days later and

https://doi.org/10.5194/egusphere-2024-3608
Preprint. Discussion started: 16 January 2025

snowoff 5 days later, shortening the snowmelt duration by 4 days. These anomalies likely reflect broader climatic drivers, such as temperature fluctuations and abnormal precipitation, affecting snowmelt dynamics in these years.

5.4.3 Change in Area Over Time

Temporal changes in area for the 'earlier' class from 1988–2023 (Fig. A5) showed no significant correlations for any snow metric. However, the Mann-Kendall Test test revealed positive and statistically significant ($p<0.05$) tau values for both snowoff and SMD, though these were modest at 0.2 and 0.25, respectively. To further examine potential trends, we segmented the data into two periods—1988–2005 and 2006–2023—and performed trend analysis on each segment independently (Figure 8).

Annual changes in the snow metric's 'earlier' class during the first half of the data record (1988-2005) identified a strong negative trend for snowmelt onset ($r = -0.65$, $p < -0.05$, $tau=-0.35$, $p < 0.05$). This implies that in the earlier years of this period, snowmelt onset was occurring earlier across the YRB relative to later years. Conversely, SMD had a strong positive trend ($r = 0.7$, $p<0.05$, $tau = 0.41$, $p <0 .05$), which suggests a longer snowmelt duration during years with earlier snowmelt onset. Snowoff exhibited no significant trends during this period, with an r value of -0.15, indicating minimal directional change.

In the second half of the data record (2006–2023), annual changes in snowmelt onset displayed a shift to a positive trend, with an r value of 0.54 ($p < 0.05$) and tau of 0.42 ($p < 0.05$). This shift suggests that snowmelt onset has been occurring progressively earlier in recent years. Snowoff during this period also exhibited a positive trend, with an r value of 0.65 ($p < 0.05$) and tau of 0.48 ($p < 0.05$), indicating an earlier occurrence of snowoff as well. Interestingly, SMD did not show any significant trends during this period due to compensating changes in snowmelt onset and snowoff timing.

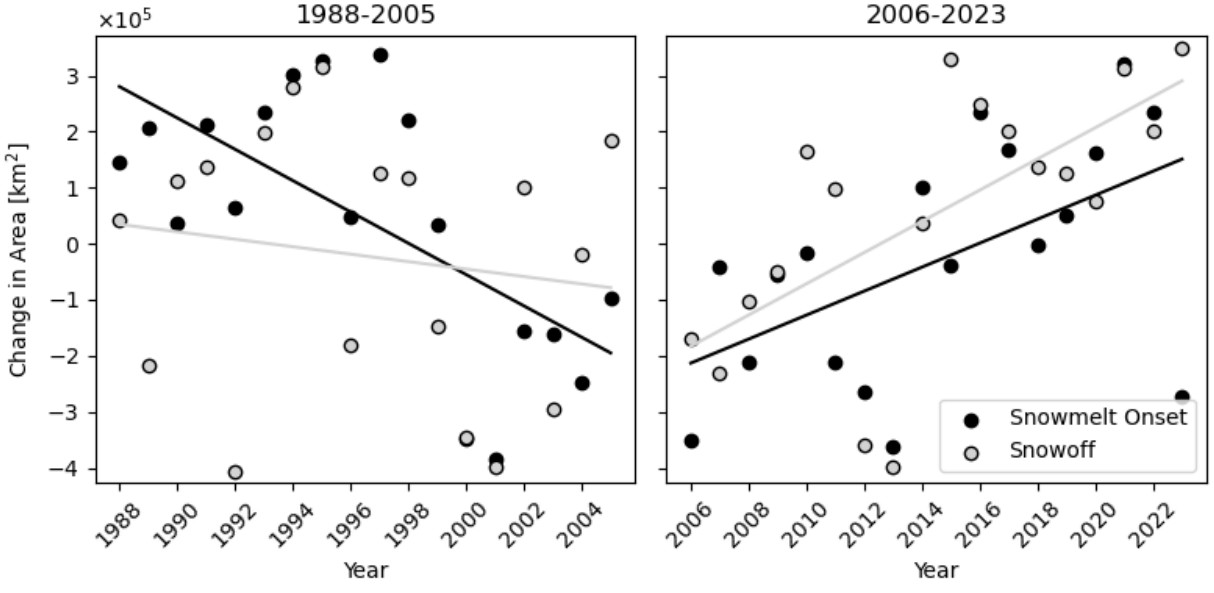

https://doi.org/10.5194/egusphere-2024-3608
Preprint. Discussion started: 16 January 2025

Figure 8: Annual changes in area between the 'earlier' climatology and the 'earlier' class for each year. The left plot shows decreasing trend for snowmelt onset but little change for snowoff from 1988-2005 while the right plot shows significant increase in change in area for both from 2006-2023.

5.5 Temperature and Snowfall Trends Across the YRB

Seasonal temperatures and annual snowfall in the YRB were analyzed using in-situ measurements from GHCNd stations. For the period 1988–2023, no significant trends were identified in Winter, Spring, Summer, or Spring/Summer temperatures, nor in annual snowfall totals. In the following sections, we present trend analysis results for annual snowfall and seasonal temperatures across the two sub-periods—1988–2005 and 2006–2023—as well as correlations with the annual snow metrics.

5.5.1 Snow depth at snowmelt onset

Between 1998 and 2005, median snow depth on the day of snowmelt onset exhibited a moderately strong negative correlation with time ($r = -0.58$, $p < 0.05$; tau = -0.40, $p < 0.05$), indicating a decrease in snowfall totals during this period (Figure 9). In contrast, from 2006 to 2023, median snow depth displayed positive and significant correlations and trends ($r = 0.68$, $p < 0.001$; tau = 0.40, $p < 0.05$). We did not examine correlations between snow depth at snowmelt onset and snow phenology metrics, as these analyses would likely introduce bias due to the use of the DOY of snowmelt onset in both training and testing datasets.

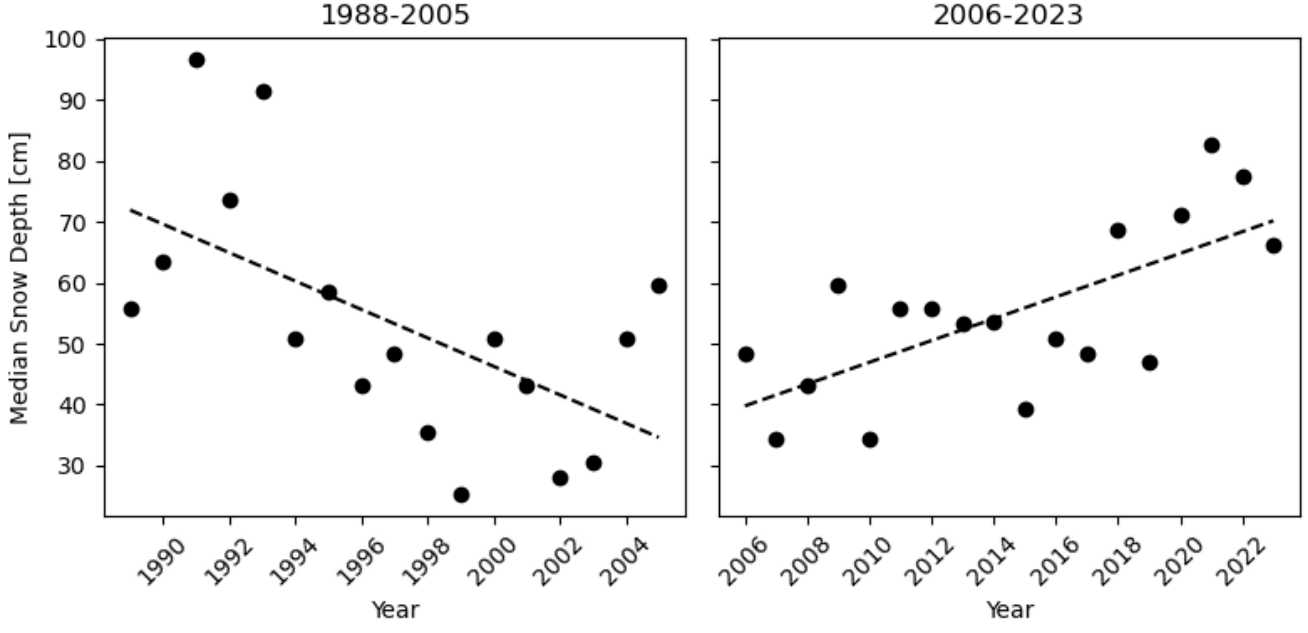

Figure 9: Harmonized median snow depth at day of snowmelt onset across the YRB as measured from GHCNd stations.

https://doi.org/10.5194/egusphere-2024-3608
Preprint. Discussion started: 16 January 2025

5.5.2 Seasonal Temperature

Trends in seasonal temperatures from 1988–2005 identified a significant increase in winter temperatures, with an r value of 0.46 ($p < 0.1$) and tau of 0.35 ($p < 0.05$). Winter temperatures were also negatively correlated with snowmelt onset ($r = -0.47$, $p < 0.05$), indicating that warmer winters were associated with earlier snowmelt. Additionally, snowoff showed a strong positive correlation with spring temperatures ($r = 0.68$, $p < 0.01$). Summer temperatures during this period were moderately correlated with both snowmelt onset and snowoff, with r values of 0.51 and 0.52 ($p < 0.1$), respectively.

From 2006–2023, no seasonal temperatures exhibited significant trends over time. However, winter and spring/summer temperatures had positive tau values of 0.33 and 0.32 ($p < 0.05$), suggesting a slight warming trend. Interestingly, snowmelt onset and snowoff were positively correlated with spring/summer temperatures, with r values of 0.48 and 0.67 ($p < 0.01$), respectively. A significant correlation was also identified between spring temperatures and snowmelt onset ($r = 0.41$, $p < 0.1$), indicating that warmer springs may contribute to earlier snowmelt.

6 Discussion

6.1 Model Performance and Limitations

The RF model classified daily snow conditions effectively, achieving high precision and recall scores, underscoring its reliability in predicting snowmelt onset and snowoff. This performance is particularly noteworthy in the complex landscape of the YRB, where traditional threshold-based methods often struggle due to heterogeneous land cover and atmospheric conditions (Pan et al., 2021). By incorporating dynamic time-series data, such as cumulative TDD and TBD, the model produced favorable predictions of snow phenology events. The inclusion of a temporal dimension within the RF framework further enabled the model to track the seasonal evolution of snow cover, enhancing model accuracy in predicting both snowmelt onset and snowoff.

In comparing bootstrapped performance metrics, the snowoff model outperformed the snowmelt onset model, a result anticipated due to the greater variability and influencing factors associated with detecting snowmelt onset. However, errors calculated by comparing in-situ observations with full model outputs showed that snowoff predictions had a higher MAE and RMSE. Notably, when RF snowoff errors were compared with errors derived from IMS and SnowModel snowoff data, they were found to be similar. This suggests that (1) accurately capturing snowoff at a single point location remains challenging due to high spatial variability at the 3.125 km spatial scale, (2) the RF snowoff model performs on par with other established snowoff datasets and (3) the uncertainties and bias in other readily available snow products.

https://doi.org/10.5194/egusphere-2024-3608
Preprint. Discussion started: 16 January 2025

The model also faces challenges related to sampling bias, due to the uneven distribution of ground-based snow depth measurements used for training and testing (Tedesco and Jeyaratnam, 2016; Tsai et al., 2019). The GHCNd stations are mostly located in accessible, lower-elevation areas and represent a very small relative area within the grid cell being evaluated. This also introduces bias into the modeled predictions for underrepresented regions, such as higher elevations or areas of higher FW in the YRB. The scarcity of in-situ observations in these areas further limits the ability of the model to generalize across different land cover types and elevations. However, emerging technologies, such as camera traps, have shown promise in measuring seasonal snow depth at varying elevations (Breen et al., 2023, 2024). These tools could expand the spatial distribution of snow measurements while reducing potential spatial bias, offering a valuable enhancement for future snow phenology studies.

We found that the RF model predicted snowmelt onset on average 3 days later than an established satellite snow phenology record derived from a Tb threshold method (Pan et al., 2020). This earlier onset predicted by the previous record is likely due to the threshold algorithm misinterpreting seasonal melt events as the main snowmelt onset. Addressing this misinterpretation was one of the primary motivations for exploring ML in snowmelt onset detection. The RF model, with its logical structure and ancillary data, is likely better equipped to distinguish between seasonal melt events and the true melt onset. Additionally, the coarser resolution of the Pan et al. (2020) dataset (6.25 km) may introduce bias by failing to capture landscape heterogeneity, particularly at higher elevations. These high-altitude areas, which are a smaller portion of the domain, tend to exhibit a lag in spring snow metrics compared to lower elevations.

The RF models showed greater uncertainty in certain YRB sub-regions, particularly at higher elevations and in coastal areas. These regions likely pose challenges due to their topographic complexity and proximity to large water bodies, which can introduce both Tb noise and variability in snowpack LWC (Du et al., 2016; Nagler and Rott, 2000). The QAQC maps, highlighted areas with higher RF prediction errors, indicate the need for refining model inputs in these regions. Incorporating higher-resolution satellite data like SAR or additional variables that account for these specific landscape characteristics would likely improve future iterations of the model and address some of the scale dependent uncertainties (Darychuk et al., 2023; Gagliano et al., 2023; Marin et al., 2020).

6.2 Implications of Changes in Snow Phenology

Annual changes in snow phenology are closely tied to current climate conditions, with snowmelt onset and snowoff generally occurring later in cooler years and earlier in warmer years. Notably, during warm years, snowmelt occurred earlier—by ~8 days—while in cooler years, the delay was ~10 days, relative to the climatology. And the difference in snowmelt onset between a warm year and cool year could be as much as 26 days. Earlier occurrence in snowmelt onset during warm years also generally translated into a longer melt duration, as noted from previous studies (Musselman et al., 2017).

https://doi.org/10.5194/egusphere-2024-3608
Preprint. Discussion started: 16 January 2025

Our analysis revealed that snowmelt onset trended toward a later date from 1988–2005, a result that might seem counterintuitive given the warming temperatures typically observed at northern latitudes. However, during this period, annual snowfall was particularly high in the beginning of this period (especially before 1994), and seasonal temperatures showed small changes. The deeper snowpack meant that more snow was available for melting earlier in the season, as reflected in the RF model outputs. This suggests that snowmelt onset is influenced more by the quantity of accumulated snow than by temperature alone (Barnett et al., 2005; Frei and Henry, 2022; Trujillo et al., 2012), except in cases of anomalously warm years, where elevated temperatures tend to override other factors (Musselman et al., 2017).

With temperatures remaining relatively stable from 1988-2005, snowoff timing followed typical seasonal patterns, explaining why we observed no significant changes during this period. Here we demonstrated the important role winter snowfall in shaping springtime snow phenology, yet trends in snowfall patterns across Alaska are complex. From 1957 to 2021, winter snowfall equivalent has increased across Alaska. However, northern and southern regions have seen a decline in snowfall during the spring and fall shoulder seasons, effectively shortening the snow cover duration (Ballinger et al., 2023).

We also showed an acceleration in both snowmelt onset and snowoff timing during the latter half of the data record (2005-2023). These changes align with recent trends in average Spring/Summer air temperature measurements in the YRB. Over the last century, Alaska has experienced varying increases in temperature across different climate divisions (Bieniek et al., 2014), with record-breaking warmth in recent years (Lara et al., 2021; Swanson et al., 2021; Walsh et al., 2017).

7 Conclusion

This study introduces an application of a RF approach to derive a 35-year snow phenology record across the YRB, delivering new insights into the timing and variability of snowmelt onset and snowoff across Alaska's largest drainage basin. Designed for enhanced delineation of spatial and temporal heterogeneity in snow metrics over more established satellite and model data records, the RF model effectively classified daily snow conditions, achieving reasonable accuracy in delineating snowmelt onset and snowoff across a highly varied landscape. By working with an improved spatial resolution of 3.125 km, the RF model was able to provide a more detailed representation of landscape features than previous Tb threshold-based snow phenology datasets, supporting more precise predictions across the YRB's diverse terrain. The enhanced spatial resolution proved especially valuable in depicting snow phenology in the region's remote, high-latitude environments, allowing the RF model to capture nuances in snowmelt timing across varying topographies, elevation ranges, and vegetation covers.

One significant advantage of the RF approach over traditional thresholding methods is its reduced sensitivity to transient melt events and atmospheric fluctuations, making it more reliable in identifying primary snowmelt onset rather than temporary thaw and early melt events caused by brief warming episodes. Additionally, the RF model's integration of dynamic predictors,

https://doi.org/10.5194/egusphere-2024-3608
Preprint. Discussion started: 16 January 2025

including cumulative thaw degree days and snow cover presence, allowed it to capture the seasonal evolution of snow conditions, while remaining less prone to errors related to isolated atmospheric warming events. However, certain challenges emerged, particularly in areas with complex topography, such as in high-elevation and coastal zones, where model prediction errors were greater. These challenges likely reflect the model's difficulty in addressing highly localized factors, like changes in snowpack liquid water content, or terrain induced microclimate variability.

As with many remote sensing models, sample bias in the RF model due to uneven ground-based data coverage poses a limitation, as in-situ snow depth measurements are predominantly collected in accessible, lower-elevation regions. This bias suggests the need for continuous updates to the in-situ training dataset, particularly by expanding measurements in higher-altitude and coastal areas within the YRB. Incorporating more extensive in-situ observations would improve the model's accuracy in underrepresented regions, allowing for a more comprehensive understanding of snow phenology across the YRB. By overcoming these current limitations and incorporating higher-resolution data sources, such as SAR, future iterations of the model could further enhance snow phenology monitoring in the YRB, making it a critical tool for understanding snow-related dynamics in response to climate change.

Finally, this study produced an extended snow phenology record spanning more than 30-years to better distinguish climate normals and quantify long-term climate trends in the YRB. By segmenting the 35-year record into two timeframes (1988–2005 and 2006–2023), we were able to detect distinct temporal trends in the spring snow metrics that corresponded with changes in seasonal temperatures and snowfall patterns. The analysis revealed that in the earlier years, snowmelt onset tended toward later dates, influenced largely by higher snowfall amounts and stable seasonal temperatures. However, in more recent years (2006–2023), both snowmelt onset and snowoff timing have advanced significantly, coinciding with rising spring and summer temperatures across the YRB. These phenological shifts, along with the lengthening of the snow-free season, align with observed patterns of earlier spring onset and more frequent anomalous warming events in recent years. The resulting snow phenology trends offer valuable insight into the YRB's changing climate and highlight the increasing influence of warming on snowpack dynamics, which hold implications for regional water availability, ecosystem health, and community resilience in the face of accelerated climate change.

8 Appendix A

Table A1. Descriptions of datasets used in this study and their sources.

Dataset	Spatial Resolution	Spatial Domain	Temporal Resolution	Period of Record	Use	Reference/Source
19 V and 19 H (K-band)	6.25 km	Northern Hemisphere	Daily	1988-Present	RF Prediction	Brodzik et al. 2018

https://doi.org/10.5194/egusphere-2024-3608
Preprint. Discussion started: 16 January 2025

37 V and 37H (Ka-band)	3.125 km	Northern Hemisphere	Daily	1988-Present	RF Prediction	Brodzik et al. 2018
Daymet	1 km	OCONUS	Daily	1980-Present	RF Prediction	Thornton et al. 1997
IMS	4 km	Northern Hemisphere	Daily	2004-Present	RF Prediction	Helfrich et al. 2007
SnowMod	3 km	Alaska and NW Canada	Daily	1980-2020	RF Prediction	Liston et al. 2023
Fractional Water (FW)	6.25 km	Alaska	Static	2003-2015	RF Prediction and Uncertainy Analysis	Du et al. 2017
Fractional Tree Cover (TC)	250 m	Alaska	Static	2011	RF Prediction and Uncertainy Analysis	Carroll et al. 2011
Elevation (GTOPO)	1 km	Alaska	Static		RF Prediction and Uncertainy Analysis	USGS
Proximity	1 km	Alaska	Static		RF Prediction and Uncertainy Analysis	GTOPO
Aspect	1 km	Alaska	Static		RF Prediction and Uncertainy Analysis	GTOPO
Glaciers	vector	Alaska/Canada	Static		Indicate permanent ice	Roberts-Pierel et al. 2022
GHCNd	in situ	Alaska	Daily	<1988-Present	RF Prediction - Testing/Training	Menne et al. 2012
MMOD	6.25 km	Alaska	Annual	1988-2018	RF Comparison	Pan et al. 2021
Snowoff	6.25 km	Alaska	Annual	1988-2018	RF Comparison	Pan et al. 2021

Table A2. Gridsearch results for RF hyper parameters.

	Snowmelt Onset	Snowoff
n_estimators	100	100
min_samples_leaf	4	4
max_depth	10	10
max_features	log2	log2
min_samples_split	5	10

https://doi.org/10.5194/egusphere-2024-3608
Preprint. Discussion started: 16 January 2025

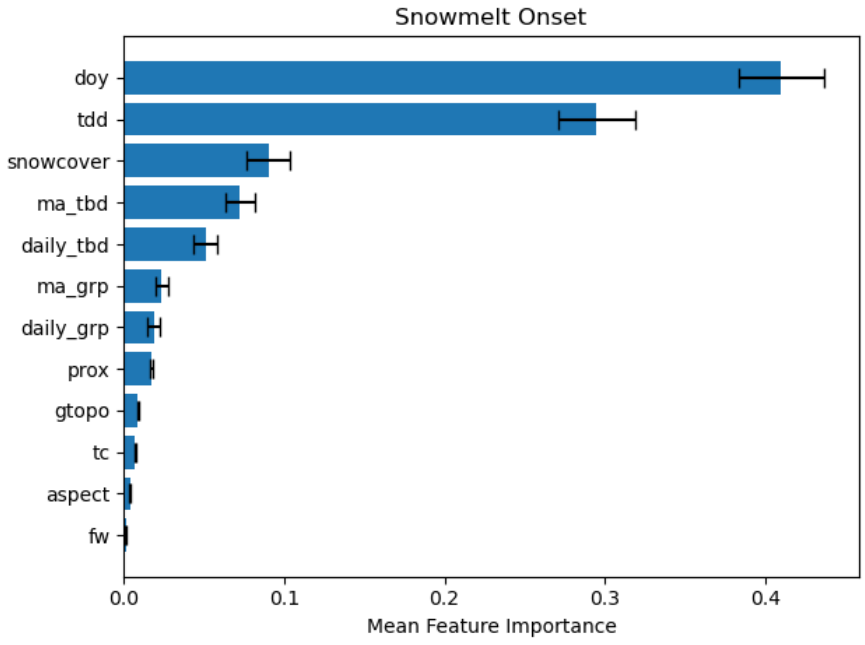

585

Figure A3. Snowmelt onset variable feature importance with +/- one standard deviation over 20 bootstrap iterations.

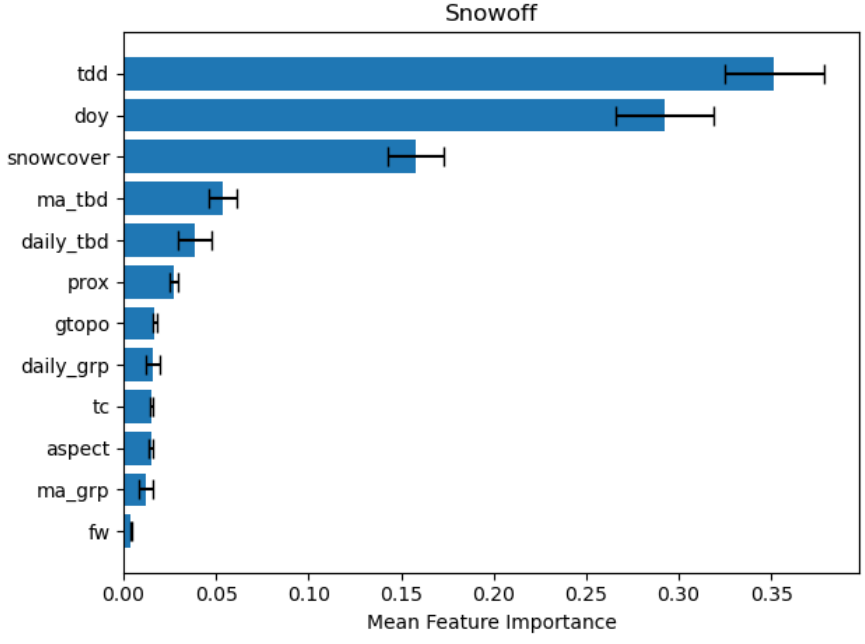

Figure A4. Snowoff variable feature importance with +/- one standard deviation over 20 bootstrap iterations.

https://doi.org/10.5194/egusphere-2024-3608
Preprint. Discussion started: 16 January 2025

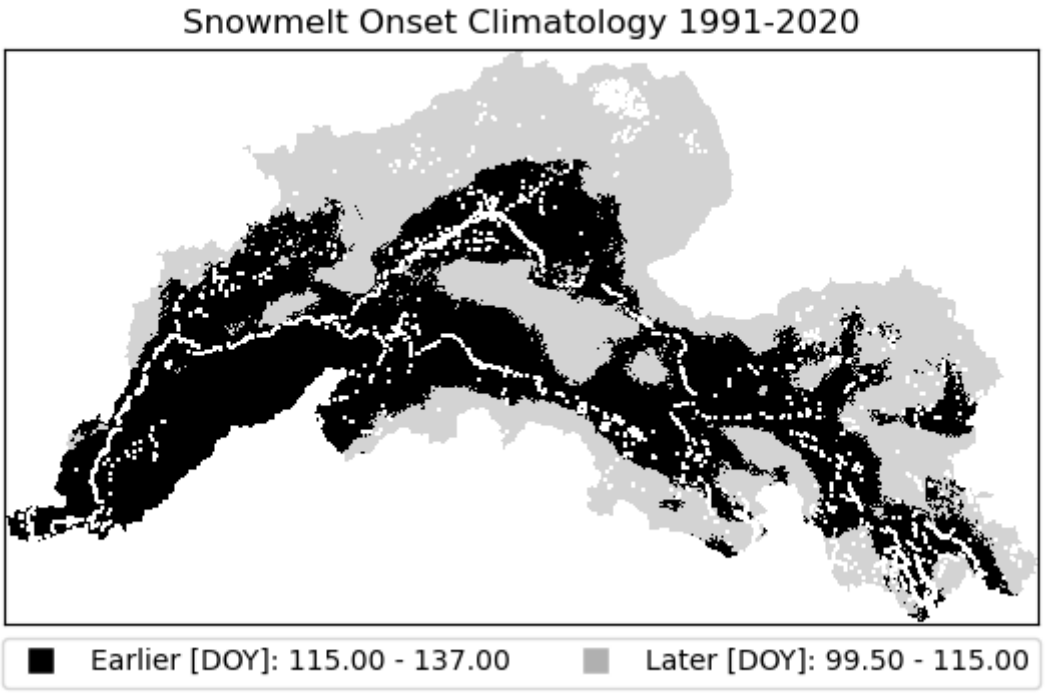

Figure A5. Snowmelt onset climatology binned into two classes, 'earlier' and 'later.' This climatology was used to assess annual changes in snowmelt onset.

Code and Data availability. Code and datasets produced in this study are available upon request.

Author Contributions. CGP wrote the manuscript. CGP processed data and analyzed the results. CGP, KL, SPG, JSK, JD, PBK contributed to the design and conceptualization. All coauthors contributed to writing and editing of the manuscript. All coauthors have read and agreed to the published version of this manuscript.

Competing interests. We declare no competing interests are present.

Acknowledgements. This research was funded by the U.S. Army Corps of Engineers, Engineer Research and Development Center (ERDC) under PE 0602146A/AT9, Project 'Tactical Geospatial Information Capabilities', Task 'Geospatial Analytics and Prediction'. Permission to publish was granted by the ERDC Public Affairs Office. Any opinions expressed in this paper are those of the authors and are not to be construed as official positions of the funding agency.

https://doi.org/10.5194/egusphere-2024-3608
Preprint. Discussion started: 16 January 2025

References

Alifu, H., Vuillaume, J.-F., Johnson, B. A., and Hirabayashi, Y.: Machine-learning classification of debris-covered glaciers using a combination of Sentinel-1/-2 (SAR/optical), Landsat 8 (thermal) and digital elevation data, Geomorphology, 369, 107365, https://doi.org/10.1016/j.geomorph.2020.107365, 2020.

Bair, E. H., Dozier, J., Rittger, K., Stillinger, T., Kleiber, W., and Davis, R. E.: How do tradeoffs in satellite spatial and temporal resolution impact snow water equivalent reconstruction?, The Cryosphere, 17, 2629–2643, https://doi.org/10.5194/tc-17-2629-2023, 2023.

Ballinger, T. J., Bhatt, U. S., Bieniek, P. A., Brettschneider, B., Lader, R. T., Littell, J. S., Thoman, R. L., Waigl, C. F., Walsh, J. E., and Webster, M. A.: Alaska Terrestrial and Marine Climate Trends, 1957–2021, Journal of Climate, 36, 4375–4391, https://doi.org/10.1175/JCLI-D-22-0434.1, 2023.

Barnett, T. P., Adam, J. C., and Lettenmaier, D. P.: Potential impacts of a warming climate on water availability in snow-dominated regions, Nature, 438, 303–309, https://doi.org/10.1038/nature04141, 2005.

Beltaos, S. and Prowse, T.: River-ice hydrology in a shrinking cryosphere, Hydrological Processes, 23, 122–144, https://doi.org/10.1002/hyp.7165, 2009.

Berger, J., Hartway, C., Gruzdev, A., and Johnson, M.: Climate Degradation and Extreme Icing Events Constrain Life in Cold-Adapted Mammals, Sci Rep, 8, 1156, https://doi.org/10.1038/s41598-018-19416-9, 2018.

Bieniek, P. A., Walsh, J. E., Thoman, R. L., and Bhatt, U. S.: Using Climate Divisions to Analyze Variations and Trends in Alaska Temperature and Precipitation, Journal of Climate, 27, 2800–2818, https://doi.org/10.1175/JCLI-D-13-00342.1, 2014.

Blandini, G., Avanzi, F., Gabellani, S., Ponziani, D., Stevenin, H., Ratto, S., Ferraris, L., and Viglione, A.: A random forest approach to quality-checking automatic snow-depth sensor measurements, The Cryosphere, 17, 5317–5333, https://doi.org/10.5194/tc-17-5317-2023, 2023.

Brabets, T., Wang, B., and Mead, R.: Environmental and hydrologic overview of the Yukon River basin, Alaska and Canada, https://doi.org/10.3133/wri994204, 2000.

Breen, C., Vuyovich, C., Odden, J., Hall, D., and Prugh, L.: Evaluating MODIS snow products using an extensive wildlife camera network, Remote Sensing of Environment, 295, 113648, https://doi.org/10.1016/j.rse.2023.113648, 2023.

Breen, C. M., Currier, W. R., Vuyovich, C., Miao, Z., and Prugh, L. R.: Snow Depth Extraction From Time-Lapse Imagery Using a Keypoint Deep Learning Model, Water Resources Research, 60, e2023WR036682, https://doi.org/10.1029/2023WR036682, 2024.

Breiman, L.: [No title found], Machine Learning, 45, 5–32, https://doi.org/10.1023/A:1010933404324, 2001.

Brodzik, M. J. and Long, D. G.: MEaSUREs Calibrated Enhanced-Resolution Passive Microwave Daily EASE-Grid 2.0 Brightness Temperature ESDR, Version 1, https://doi.org/10.5067/MEASURES/CRYOSPHERE/NSIDC-0630.001, 2016.

https://doi.org/10.5194/egusphere-2024-3608
Preprint. Discussion started: 16 January 2025

Brodzik, M. J., Long, D. G., and Hardman, M. A.: Best Practices in Crafting the Calibrated, Enhanced-Resolution Passive-Microwave EASE-Grid 2.0 Brightness Temperature Earth System Data Record, Remote Sensing, 10, 1793, https://doi.org/10.3390/rs10111793, 2018.

Brown, D. R. N., Brinkman, T. J., Bolton, W. R., Brown, C. L., Cold, H. S., Hollingsworth, T. N., and Verbyla, D. L.: Implications of climate variability and changing seasonal hydrology for subarctic riverbank erosion, Climatic Change, 162, 1–20, https://doi.org/10.1007/s10584-020-02748-9, 2020.

Callaghan, T. V., Johansson, M., Brown, R. D., Groisman, P. Ya., Labba, N., Radionov, V., Barry, R. G., Bulygina, O. N., Essery, R. L. H., Frolov, D. M., Golubev, V. N., Grenfell, T. C., Petrushina, M. N., Razuvaev, V. N., Robinson, D. A., Romanov, P., Shindell, D., Shmakin, A. B., Sokratov, S. A., Warren, S., and Yang, D.: The Changing Face of Arctic Snow Cover: A Synthesis of Observed and Projected Changes, AMBIO, 40, 17–31, https://doi.org/10.1007/s13280-011-0212-y, 2011.

Campbell, S. W., Briggs, M., Roy, S. G., Douglas, T. A., and Saari, S.: Ground-penetrating radar, electromagnetic induction, terrain, and vegetation observations coupled with machine learning to map permafrost distribution at Twelvemile Lake, Alaska, Permafrost & Periglacial, 32, 407–426, https://doi.org/10.1002/ppp.2100, 2021.

Cold, H. S., Brinkman, T. J., Brown, C. L., Hollingsworth, T. N., Brown, D. R. N., and Heeringa, K. M.: Assessing vulnerability of subsistence travel to effects of environmental change in Interior Alaska, E&S, 25, art20, https://doi.org/10.5751/ES-11426-250120, 2020.

Cosgrove, C. L., Wells, J., Nolin, A. W., Putera, J., and Prugh, L. R.: Seasonal influence of snow conditions on Dall's sheep productivity in Wrangell-St Elias National Park and Preserve, PLoS ONE, 16, e0244787, https://doi.org/10.1371/journal.pone.0244787, 2021.

Darychuk, S. E., Shea, J. M., Menounos, B., Chesnokova, A., Jost, G., and Weber, F.: Snowmelt characterization from optical and synthetic-aperture radar observations in the La Joie Basin, British Columbia, The Cryosphere, 17, 1457–1473, https://doi.org/10.5194/tc-17-1457-2023, 2023.

Dattler, M. E., Medley, B., and Stevens, C. M.: A physics-based Antarctic melt detection technique: combining Advanced Microwave Scanning Radiometer 2, radiative-transfer modeling, and firn modeling, The Cryosphere, 18, 3613–3631, https://doi.org/10.5194/tc-18-3613-2024, 2024.

Derksen, C. and Brown, R.: Spring snow cover extent reductions in the 2008–2012 period exceeding climate model projections, Geophysical Research Letters, 39, 2012GL053387, https://doi.org/10.1029/2012GL053387, 2012.

Dolant, C., Langlois, A., Montpetit, B., Brucker, L., Roy, A., and Royer, A.: Development of a rain-on-snow detection algorithm using passive microwave radiometry, Hydrological Processes, 30, 3184–3196, https://doi.org/10.1002/hyp.10828, 2016.

Du, J., Kimball, J. S., Jones, L. A., and Watts, J. D.: Implementation of satellite based fractional water cover indices in the pan-Arctic region using AMSR-E and MODIS, Remote Sensing of Environment, 184, 469–481, https://doi.org/10.1016/j.rse.2016.07.029, 2016.

Du, J., Kimball, J. S., Jones, L. A., Kim, Y., Glassy, J., and Watts, J. D.: A global satellite environmental data record derived from AMSR-E and AMSR2 microwave Earth observations, Earth Syst. Sci. Data, 9, 791–808, https://doi.org/10.5194/essd-9-791-2017, 2017.

https://doi.org/10.5194/egusphere-2024-3608
Preprint. Discussion started: 16 January 2025

Dunmire, D., Lievens, H., Boeykens, L., and De Lannoy, G. J. M.: A machine learning approach for estimating snow depth across the European Alps from Sentinel-1 imagery, Remote Sensing of Environment, 314, 114369, https://doi.org/10.1016/j.rse.2024.114369, 2024.

Frei, E. R. and Henry, G. H. R.: Long-term effects of snowmelt timing and climate warming on phenology, growth, and reproductive effort of Arctic tundra plant species, Arctic Science, 8, 700–721, https://doi.org/10.1139/as-2021-0028, 2022.

Gagliano, E., Shean, D., Henderson, S., and Vanderwilt, S.: Capturing the Onset of Mountain Snowmelt Runoff Using Satellite Synthetic Aperture Radar, Geophysical Research Letters, 50, e2023GL105303, https://doi.org/10.1029/2023GL105303, 2023.

Grenfell, T. C. and Putkonen, J.: A method for the detection of the severe rain-on-snow event on Banks Island, October 2003, using passive microwave remote sensing, Water Resources Research, 44, 2007WR005929, https://doi.org/10.1029/2007WR005929, 2008.

Guidicelli, M., Huss, M., Gabella, M., and Salzmann, N.: Spatio-temporal reconstruction of winter glacier mass balance in the Alps, Scandinavia, Central Asia and western Canada (1981–2019) using climate reanalyses and machine learning, The Cryosphere, 17, 977–1002, https://doi.org/10.5194/tc-17-977-2023, 2023.

Helfrich, S. R., McNamara, D., Ramsay, B. H., Baldwin, T., and Kasheta, T.: Enhancements to, and forthcoming developments in the Interactive Multisensor Snow and Ice Mapping System (IMS), Hydrological Processes, 21, 1576–1586, https://doi.org/10.1002/hyp.6720, 2007.

Jääskeläinen, E., Manninen, T., Hakkarainen, J., and Tamminen, J.: Filling gaps of black-sky surface albedo of the Arctic sea ice using gradient boosting and brightness temperature data, International Journal of Applied Earth Observation and Geoinformation, 107, 102701, https://doi.org/10.1016/j.jag.2022.102701, 2022.

Kim, Y., Kimball, J. S., McDonald, K. C., and Glassy, J.: Developing a Global Data Record of Daily Landscape Freeze/Thaw Status Using Satellite Passive Microwave Remote Sensing, IEEE Trans. Geosci. Remote Sensing, 49, 949–960, https://doi.org/10.1109/TGRS.2010.2070515, 2011.

Kim, Y., Kimball, J. S., Glassy, J., and Du, J.: An extended global Earth system data record on daily landscape freeze–thaw status determined from satellite passive microwave remote sensing, 2017.

Lara, M. J., Chen, Y., and Jones, B. M.: Recent warming reverses forty-year decline in catastrophic lake drainage and hastens gradual lake drainage across northern Alaska, Environ. Res. Lett., 16, 124019, https://doi.org/10.1088/1748-9326/ac3602, 2021.

Lesack, L. F. W., Marsh, P., Hicks, F. E., and Forbes, D. L.: Local spring warming drives earlier river-ice breakup in a large Arctic delta, Geophysical Research Letters, 41, 1560–1567, https://doi.org/10.1002/2013GL058761, 2014.

Ling, F. and Zhang, T.: Impact of the timing and duration of seasonal snow cover on the active layer and permafrost in the Alaskan Arctic, Permafrost & Periglacial, 14, 141–150, https://doi.org/10.1002/ppp.445, 2003.

Long, D. G. and Brodzik, M. J.: Optimum Image Formation for Spaceborne Microwave Radiometer Products, IEEE Trans. Geosci. Remote Sensing, 54, 2763–2779, https://doi.org/10.1109/TGRS.2015.2505677, 2016.

Marin, C., Bertoldi, G., Premier, V., Callegari, M., Brida, C., Hürkamp, K., Tschiersch, J., Zebisch, M., and Notarnicola, C.: Use of Sentinel-1 radar observations to evaluate snowmelt dynamics in alpine regions, The Cryosphere, 14, 935–956, https://doi.org/10.5194/tc-14-935-2020, 2020.

https://doi.org/10.5194/egusphere-2024-3608
Preprint. Discussion started: 16 January 2025

Menne, M. J., Durre, I., Vose, R. S., Gleason, B. E., and Houston, T. G.: An Overview of the Global Historical Climatology Network-Daily Database, Journal of Atmospheric and Oceanic Technology, 29, 897–910, https://doi.org/10.1175/JTECH-D-11-00103.1, 2012.

Musselman, K. N., Clark, M. P., Liu, C., Ikeda, K., and Rasmussen, R.: Slower snowmelt in a warmer world, Nature Clim Change, 7, 214–219, https://doi.org/10.1038/nclimate3225, 2017.

Nagler, T. and Rott, H.: Retrieval of wet snow by means of multitemporal SAR data, IEEE Trans. Geosci. Remote Sensing, 38, 754–765, https://doi.org/10.1109/36.842004, 2000.

Niittynen, P., Heikkinen, R. K., and Luoto, M.: Snow cover is a neglected driver of Arctic biodiversity loss, Nature Clim Change, 8, 997–1001, https://doi.org/10.1038/s41558-018-0311-x, 2018.

Pan, C. G., Kirchner, P. B., Kimball, J. S., Kim, Y., and Du, J.: Rain-on-snow events in Alaska, their frequency and distribution from satellite observations, Environ. Res. Lett., 13, 075004, https://doi.org/10.1088/1748-9326/aac9d3, 2018.

Pan, C. G., Kirchner, P. B., Kimball, J. S., and Du, J.: A Long-Term Passive Microwave Snowoff Record for the Alaska Region 1988–2016, Remote Sensing, 12, 153, https://doi.org/10.3390/rs12010153, 2020.

Pan, C. G., Kirchner, P. B., Kimball, J. S., Du, J., and Rawlins, M. A.: Snow Phenology and Hydrologic Timing in the Yukon River Basin, AK, USA, Remote Sensing, 13, 2284, https://doi.org/10.3390/rs13122284, 2021.

Pedregosa, F., Pedregosa, F., Varoquaux, G., Varoquaux, G., Org, N., Gramfort, A., Gramfort, A., Michel, V., Michel, V., Fr, L., Thirion, B., Thirion, B., Grisel, O., Grisel, O., Blondel, M., Prettenhofer, P., Prettenhofer, P., Weiss, R., Dubourg, V., Dubourg, V., Vanderplas, J., Passos, A., Tp, A., and Cournapeau, D.: Scikit-learn: Machine Learning in Python, MACHINE LEARNING IN PYTHON, 2011.

Pulliainen, J., Aurela, M., Laurila, T., Aalto, T., Takala, M., Salminen, M., Kulmala, M., Barr, A., Heimann, M., Lindroth, A., Laaksonen, A., Derksen, C., Mäkelä, A., Markkanen, T., Lemmetyinen, J., Susiluoto, J., Dengel, S., Mammarella, I., Tuovinen, J.-P., and Vesala, T.: Early snowmelt significantly enhances boreal springtime carbon uptake, Proc. Natl. Acad. Sci. U.S.A., 114, 11081–11086, https://doi.org/10.1073/pnas.1707889114, 2017.

Ramage, J. M. and Isacks, B. L.: Determination of melt-onset and refreeze timing on southeast Alaskan icefields using SSM/I diurnal amplitude variations, Ann. Glaciol., 34, 391–398, https://doi.org/10.3189/172756402781817761, 2002.

Rantanen, M., Karpechko, A. Yu., Lipponen, A., Nordling, K., Hyvärinen, O., Ruosteenoja, K., Vihma, T., and Laaksonen, A.: The Arctic has warmed nearly four times faster than the globe since 1979, Commun Earth Environ, 3, 168, https://doi.org/10.1038/s43247-022-00498-3, 2022.

Rees, A., Lemmetyinen, J., Derksen, C., Pulliainen, J., and English, M.: Observed and modelled effects of ice lens formation on passive microwave brightness temperatures over snow covered tundra, Remote Sensing of Environment, 114, 116–126, https://doi.org/10.1016/j.rse.2009.08.013, 2010.

Rittger, K., Krock, M., Kleiber, W., Bair, E. H., Brodzik, M. J., Stephenson, T. R., Rajagopalan, B., Bormann, K. J., and Painter, T. H.: Multi-sensor fusion using random forests for daily fractional snow cover at 30 m, Remote Sensing of Environment, 264, 112608, https://doi.org/10.1016/j.rse.2021.112608, 2021.

Roberts-Pierel, B. M., Kirchner, P. B., Kilbride, J. B., and Kennedy, R. E.: Glacier Covered Area for the State of Alaska, 1985-2020, https://doi.org/10.7265/8ESQ-W553, 2022.

https://doi.org/10.5194/egusphere-2024-3608
Preprint. Discussion started: 16 January 2025

Scholten, R. C., Jandt, R., Miller, E. A., Rogers, B. M., and Veraverbeke, S.: Overwintering fires in boreal forests, Nature, 593, 399–404, https://doi.org/10.1038/s41586-021-03437-y, 2021.

Semmens, K. A. and Ramage, J. M.: Recent changes in spring snowmelt timing in the Yukon River basin detected by passive microwave satellite data, The Cryosphere, 7, 905–916, https://doi.org/10.5194/tc-7-905-2013, 2013.

Swanson, D. K., Sousanes, P. J., and Hill, K.: Increased mean annual temperatures in 2014–2019 indicate permafrost thaw in Alaskan national parks, Arctic, Antarctic, and Alpine Research, 53, 1–19, https://doi.org/10.1080/15230430.2020.1859435, 2021.

Tedesco, M. and Jeyaratnam, J.: A New Operational Snow Retrieval Algorithm Applied to Historical AMSR-E Brightness Temperatures, Remote Sensing, 8, 1037, https://doi.org/10.3390/rs8121037, 2016.

Tedesco, M. and Miller, J.: Observations and statistical analysis of combined active–passive microwave space-borne data and snow depth at large spatial scales, Remote Sensing of Environment, 111, 382–397, https://doi.org/10.1016/j.rse.2007.04.019, 2007.

Tedesco, M., Pulliainen, J., Takala, M., Hallikainen, M., and Pampaloni, P.: Artificial neural network-based techniques for the retrieval of SWE and snow depth from SSM/I data, Remote Sensing of Environment, 90, 76–85, https://doi.org/10.1016/j.rse.2003.12.002, 2004.

Tedesco, M., Mote, T., Steffen, K., Hall, D. K., and Abdalati, W.: Remote sensing of melting snow and ice, in: Remote Sensing of the Cryosphere, edited by: Tedesco, M., Wiley, 99–122, https://doi.org/10.1002/9781118368909.ch6, 2015.

Thornton, P. E., Shrestha, R., Thornton, M., Kao, S.-C., Wei, Y., and Wilson, B. E.: Gridded daily weather data for North America with comprehensive uncertainty quantification, Sci Data, 8, 190, https://doi.org/10.1038/s41597-021-00973-0, 2021.

Trujillo, E., Molotch, N. P., Goulden, M. L., Kelly, A. E., and Bales, R. C.: Elevation-dependent influence of snow accumulation on forest greening, Nature Geosci, 5, 705–709, https://doi.org/10.1038/ngeo1571, 2012.

Tsai, Y.-L., Dietz, A., Oppelt, N., and Kuenzer, C.: Wet and Dry Snow Detection Using Sentinel-1 SAR Data for Mountainous Areas with a Machine Learning Technique, Remote Sensing, 11, 895, https://doi.org/10.3390/rs11080895, 2019.

Walsh, J. E., Bieniek, P. A., Brettschneider, B., Euskirchen, E. S., Lader, R., and Thoman, R. L.: The Exceptionally Warm Winter of 2015/16 in Alaska, Journal of Climate, 30, 2069–2088, https://doi.org/10.1175/JCLI-D-16-0473.1, 2017.

Wang, L., Derksen, C., Brown, R., and Markus, T.: Recent changes in pan-Arctic melt onset from satellite passive microwave measurements, Geophysical Research Letters, 40, 522–528, https://doi.org/10.1002/grl.50098, 2013.

Wang, L., Toose, P., Brown, R., and Derksen, C.: Frequency and distribution of winter melt events from passive microwavesatellite data in the pan-Arctic, 1988–2013, The Cryosphere, 10, 2589–2602, https://doi.org/10.5194/tc-10-2589-2016, 2016.